

High Performance UWB MIMO Antenna by Using Neutralization Line Technique

Aziz Dkiouak^{1, *}, Mohssine El Ouahabi¹, Saad Chakkor², Mostafa Baghour³,
Alia Zakriti¹, and Youssef Lagmich⁴

Abstract—In this work, we propose a compact CoPlanar Waveguide (CPW) fed two-port multiple-input multiple-output (MIMO) antenna with high isolation for Ultra-Wideband (UWB) applications. The proposed antenna consisting of two symmetrical radiators placed side-by-side on an FR-4 substrate with a size of $0.48\lambda \times 0.48\lambda \times 0.01\lambda \text{ mm}^3$ at 3.1 GHz (where $\lambda =$ guided wavelength at the lowest frequency of operation). The isolation between the antenna elements is more than 16.5 dB in the entire UWB, which is achieved by introducing in the ground plane a vertical T-shaped neutralization line. The simulation results of the antenna system are in good agreement with the measured one. The proposed antenna covers the entire UWB with an impedance bandwidth 8.6 GHz (from 3.1 to 11.7 GHz), considering the -10 dB standard. The designed UWB MIMO antenna has a low envelope correlation coefficient (less than 0.57), a good efficiency (more than 50%), a low total channel capacity loss ($CCL_{Total} < 0.25$ bit/s/Hz), and stable total active reflection coefficient (TARC) attributes, thus meeting the standards applicable to various wireless MIMO applications.

1. INTRODUCTION

In wireless communication system, the antenna, as an important component, is mainly used for receiving and transmitting signals, and its performance largely determines the normal communication of the whole system. Ultra-Wideband (UWB) technology is a new communication technology that is very different from traditional communication one. Instead of using carriers from traditional communication systems, it transmits data by sending and receiving very narrow pulses of nanoseconds or less, resulting in bandwidths of the order of GHz. This technology has the advantages of wide bandwidth (3.1–10.6 GHz), high penetration, high security, low system complexity, the ability to provide precise positioning accuracy but a low power spectral density, which will cause multipath fading problem [1]. This problem can be converted into advantages and exploited by using Multiple Input Multiple Output (MIMO) technology [2]. The combination of UWB technology and MIMO technology is beneficial for the development of current communication technology [3, 4].

This system uses multiple antennas, for which it is necessary to maintain a low mutual coupling between the antenna elements to enhance their diversity performance. Many publications have reported various techniques to minimize the mutual coupling between MIMO UWB antennas. In [5], a thin vertical neutralization line is added between the two patches to reinforce the isolation over the entire band and achieves a wideband decoupling current. In [6], an inverse L-shaped stub is inserted in the ground plane of the antenna to diminish mutual coupling amid antenna elements. A compact dual-band

Received 11 January 2023, Accepted 10 March 2023, Scheduled 27 March 2023

* Corresponding author: Aziz Dkiouak (dkiouakaziz@hotmail.fr).

¹ Sciences and Advanced Technologies Team, ENSA of Tetuan, Abdelmalek Essaadi University, Tetuan, Morocco. ² LabTIC Laboratory, ENSA of Tangier, Abdelmalek Essaadi University, Tangier, Morocco. ³ Smart Materials and Artificial intelligence Team, LCCPS Laboratory, ENSAM of Casablanca, Hassan II University, Casablanca, Morocco. ⁴ Laboratory of Sciences and Advanced Technologies Polydisciplinary, Faculty of Larache, Abdelmalek Essaadi University, Larache, Morocco.

MIMO antenna with high isolation by using orthogonal polarization is proposed in [7]. El Ouahabi et al. [8] designed a compact MIMO antenna by combining the orthogonal microstrip line and a single complementary split ring resonator (S-CSRR) to achieve high isolation over the operating bands of the proposed structure.

Several studies have designed MIMO antennas with high isolation, small size, and low envelope correlation coefficient (ECC). In [9], a wideband flexible/transparent connected-ground MIMO antenna is proposed for sub-6 GHz 5G and WLAN applications. A transparent 2-element 5G MIMO antenna for sub-6 GHz applications has been proposed in [10].

In this paper, two compact UWB MIMO antennas with good performance are proposed. A vertical T-shaped neutralization line technique has been used between two elements to achieve a high isolation of more than 16.5 dB across the band. The UWB MIMO performance is analyzed and evaluated by envelope correlation coefficient, efficiency, total active reflection coefficient, and total channel capacity loss.

2. ANTENNA DESIGN

2.1. Antenna Geometry

The final design of the UWB MIMO antenna geometry using the CPW technology and spatial diversity is shown in Figure 1. The antenna is printed on an FR-4 substrate with a thickness h of 1.6 mm, a relative permittivity ϵ_r of 4.4, and a loss tangent δ of 0.02. This substrate is available in our laboratory that makes the fabrication of prototypes possible, in addition to its low cost compared to other types

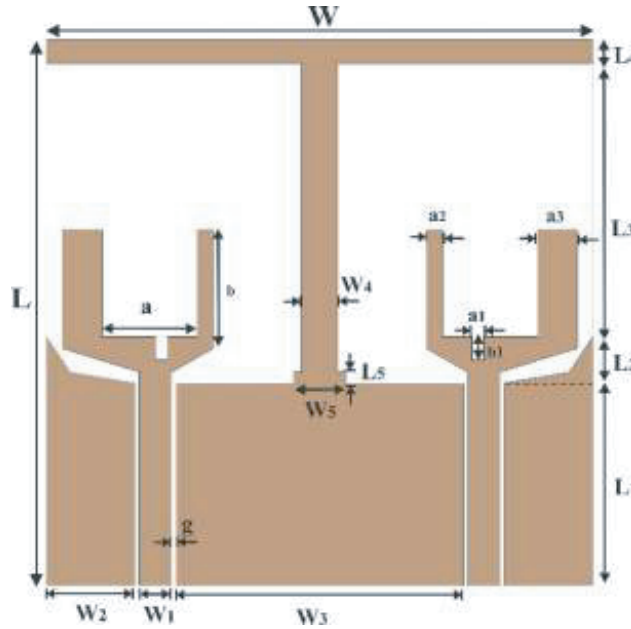


Figure 1. The proposed UWB MIMO antenna configurations.

Table 1. Dimensions of the UWB MIMO antenna in (mm).

Parameters	W	L	W_1	W_2	W_3	W_4	W_5	L_1	L_2	L_3
Values	46	46	2.7	7.41	24.16	4.4	3	17	4	23
Parameters	L_4	L_5	a_1	a_2	a_3	g	a	b	b_1	
Values	2	1	1	1.35	3.35	0.4	8	9	2	

of substrates. The two antenna elements are placed in parallel to each other and separated by a vertical T-shaped neutralization line to enhance the isolation over the entire band. The two modified rectangular radiators with a partial ground plane are independently fed by a CPW 50 ohm feed line. The designed antenna dimensions are simulated and optimized by the electromagnetic simulation software CST. Finally, the optimized dimensions of the UWB MIMO antenna are listed in Table 1.

2.2. Effect of the Vertical T-Shaped Neutralization Line on the S -Parameters

The simulated S -parameters of the UWB MIMO antenna with and without the T-shaped neutralization line are shown in Figure 2. Because of the symmetry, only the reflection coefficient S_{11} and the isolation coefficient S_{21} are given. The purpose of inserting this metallic line is to compensate the existence of the electromagnetic field in the suggested structure at the UWB. This technique improves the isolation between the radiators of the antenna and therefore improves other parameters characterizing the MIMO UWB antenna.

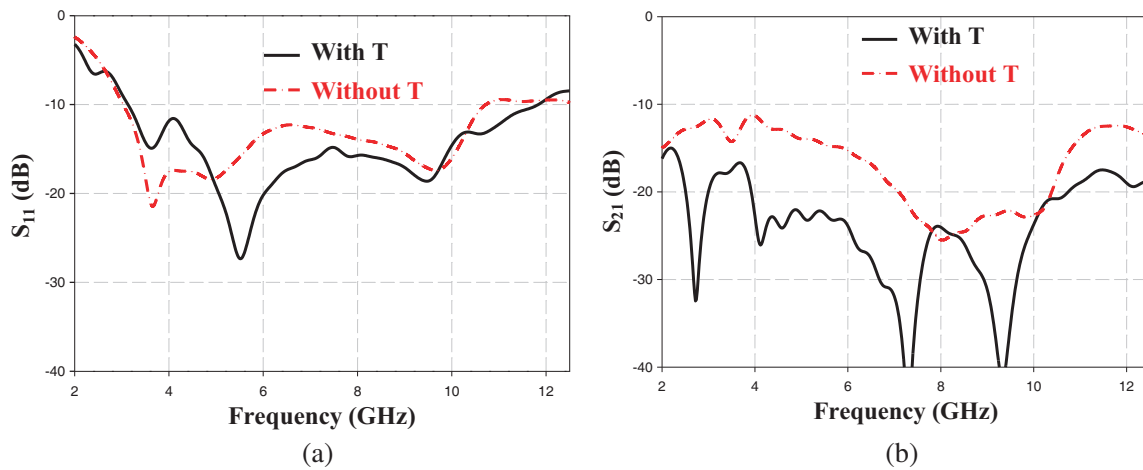


Figure 2. The simulated S -parameters with and without vertical T-shaped neutralization line. (a) S_{11} , (b) S_{21} .

By observing this figure, it is clear that the effect of the metal line is very important on bandwidth enhancement (more than 1 GHz), especially at the higher part (Figure 2(a)). We also notice that in the same figure, the adaptation is enhanced at the level of the frequency range [5.117 GHz]. In addition, without vertical T-shaped neutralization line structure, the isolation between two elements is 11.20 dB. By introducing it in ground plane, the isolation value is improved and becomes 16.50 dB. It may be concluded that the addition of the metallic line significantly contributes to the improvement of the isolation in the whole band of 3.5 dB and above, as shown in Figure 2(b).

3. RESULT ANALYSIS

3.1. Fabrication and Measurement

To check the performance of the UWB MIMO antenna operation, we process and test the MIMO antenna according to the final optimized dimensions. CSTMWS software is utilized to simulate the proposed antenna. The suggested structure is fabricated using LPKF protomat E33 machine as shown in Figure 3(a). The measurements of the scattering parameters are conducted with a Rohde and Schwarz ZVB 20 vector network analyser with a range of of 20 GHz (Figure 3(b)). The fabrication process is carried out at AbdelMaleK Essaâdi University Laboratories.

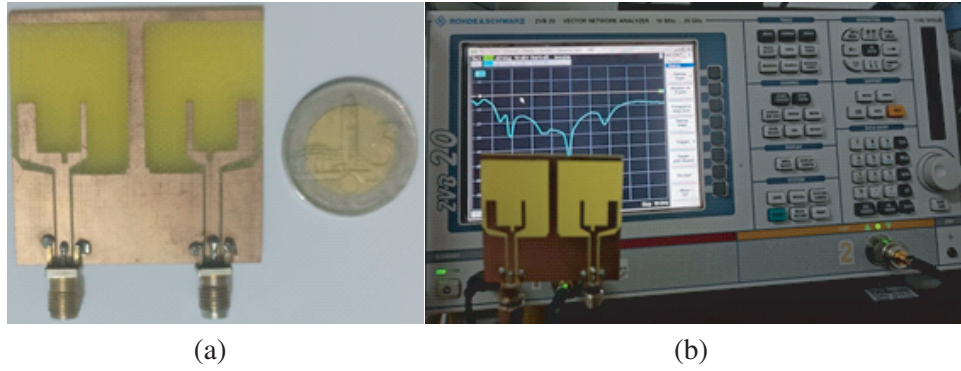


Figure 3. (a) Antenna prototype photograph and (b) picture during S -parameters measurement.

3.2. S -Parameter

Figure 4 displays the measured and simulated S -parameters of the presented UWB MIMO antenna. As we can see from this figure, there is a good agreement between the two results, but there are some deviations. The minor variation between simulated and tested results is because of losses due to solder SMA connectors, the error in the manufacturing, and measurement process. The simulated and measured bandwidths of the tested MIMO antenna are 8.6 GHz going from 3.1 to 11.7 GHz and about 9.68 GHz ranging from 2.70 to 12.38 GHz, respectively, which can be used for UWB applications. Across the impedance bandwidth, the simulated and measured isolation values of the presented UWB MIMO antenna are 16.5 dB and 16.2 dB, respectively. Table 2 summarizes the simulated and measured results of the proposed antenna.

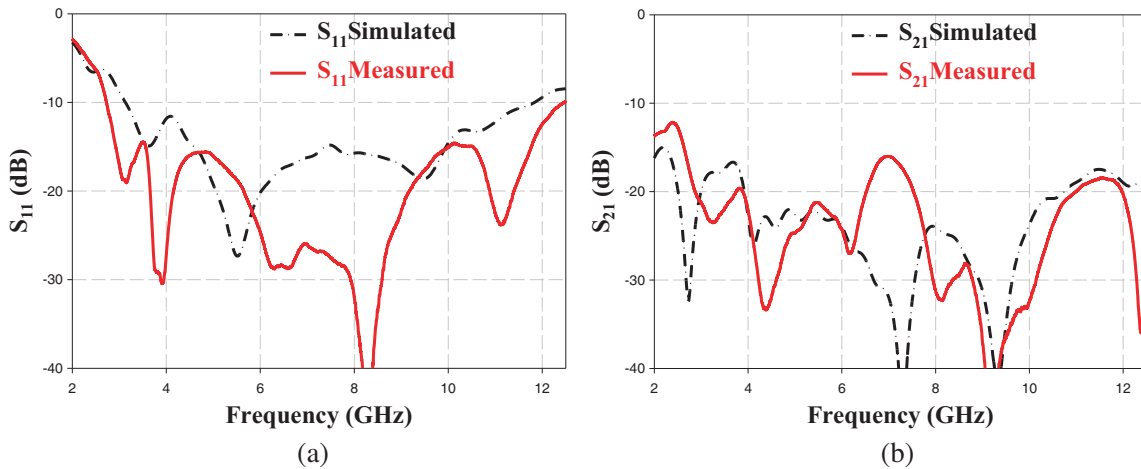


Figure 4. Simulated and measured reflection coefficient (S_{11}) and transmission coefficient (S_{21}): (a) S_{11} and (b) S_{21} .

3.3. Surface Current Distribution

In order to study the performance of the structure, surface currents on the radiating patch, ground plane, and feedline at three resonances of 4.1, 7.3, and 9.8 GHz are simulated as depicted in Figure 5. Due to the symmetry of the antenna, when port 1 is energized, the other port terminates with a $50\ \Omega$ load. From this figure, the adjacent element receives only a small surface current when the first element of the studied antenna is excited. Beside, the surface current distribution is dominant at the excited radiator, ground plane, and the vertical T-shaped neutralization line. This line forces the current to

Table 2. Performance comparisons between simulated and measured results of the UWB MIMO antenna.

Proposed MIMO antenna	UWB		
	BW range (GHz)	BW (GHz)	Isolation (dB)
Measured	2.70 to 12.38	9.68	16.2
Simulated	3.1 to 11.7	8.6	16.5

BW: Bandwidth

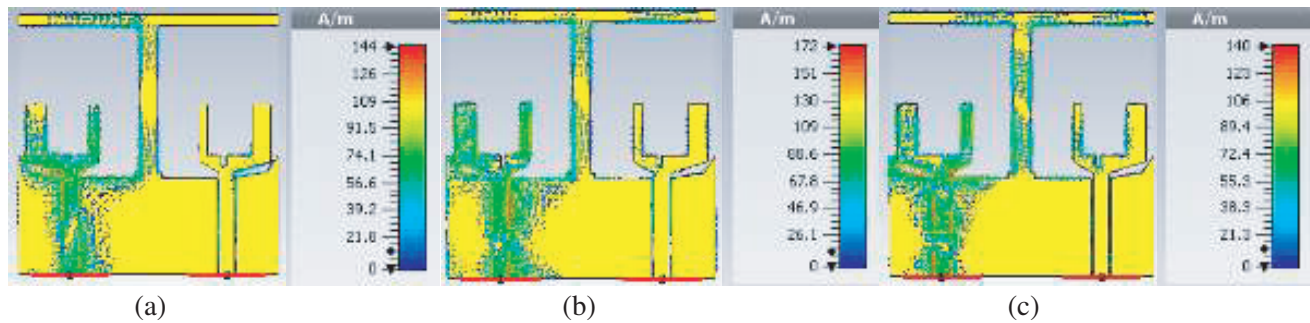


Figure 5. The surface current distribution of the UWB MIMO antenna at: (a) 4.1 GHz, (b) 7.3 GHz, (c) 9.8 GHz.

concentrate on the excited port and the ground plane of the structure, instead of moving directly from the excited port to the other one. The purpose of this technique is to increase the effective path length of the surface current, which minimizes the mutual coupling in the presented MIMO antenna.

Figure 5(a) illustrates that the current is uniformly distributed over the entire excited patch and a part of the vertical T-shaped neutralization line (half the T-line) with a high current at 4.1 GHz of 144 A/m (about 43.15 dB). Figure 5(b) displays a high current at 7.3 GHz of 170 A/m (about 44.71 dB) concentrated on the excited antenna and the vertical T-shaped neutralization line. At 9.8 GHz, Figure 5(c) shows that a high current of 140 A/m (about 4.95 dB) is present on the excited antenna, the vertical T-shaped neutralization line and a small current flow through to the other patch due to the high frequency effect.

3.4. Radiation Direction Diagram

Figure 6 shows the simulated and measured radiation patterns of the UWB MIMO antenna at 3.6 GHz, 6 GHz, and 9.8 GHz. Because of symmetry, the proposed UWB MIMO antenna was only measured when port one is excited and the other terminated with a 50 Ω load. It can be seen that the antenna has good radiation characteristics: omnidirectional “O” shape in the *H*-plane but slightly distorted and nearly bidirectional in the *E*-plane “8” shape (similar to that of the traditional monopole antenna), indicating that the MIMO antenna is suitable for receiving and transmitting signals in all directions in order to realize the multiple input and multiple output function.

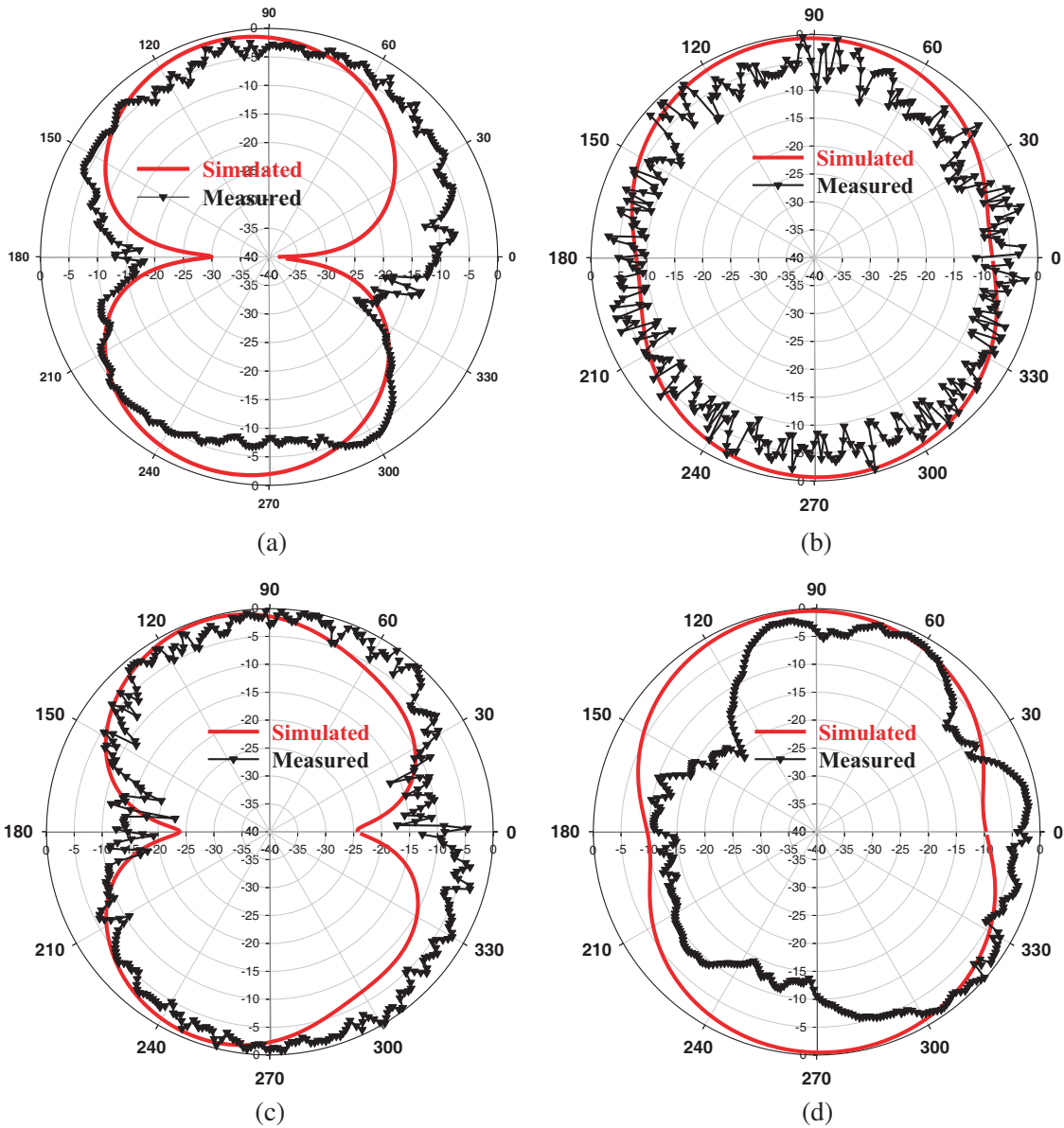
3.5. Radiation Efficiency

Figure 7 is the result of the radiation efficiency of the MIMO antenna as a function of frequency. It can be seen from the figure that the antenna has a good radiation efficiency in the UWB, all above 50%. At high frequency range (especially from 10.4 to 11.7 GHz), the radiation efficiency decreases quickly from 59% to 48% due to the dielectric loss in the FR4 substrate.

3.6. Diversity Characterization

For MIMO antennas, the envelope correlation coefficient (ECC) is used to illustrate the correlation between MIMO antenna units. A lower ECC indicates a higher diversity gain. The ECC calculated using the S -parameter (Eq. (1)) is approximated as an ideal uniform scattering environment [11, 12]. In order to obtain calculation results that reflect the actual situation, the ECC was calculated numerically using the far-field radiation direction map according to equation (Eq. (2)) [13, 14].

$$ECC = \frac{\left| \sum_{n=1}^N S_{i,n}^* S_{n,j} \right|^2}{\prod_{k=i,j} \left[1 - \left| \sum_{n=1}^N S_{i,n}^* S_{n,k} \right|^2 \right]} \quad (1)$$



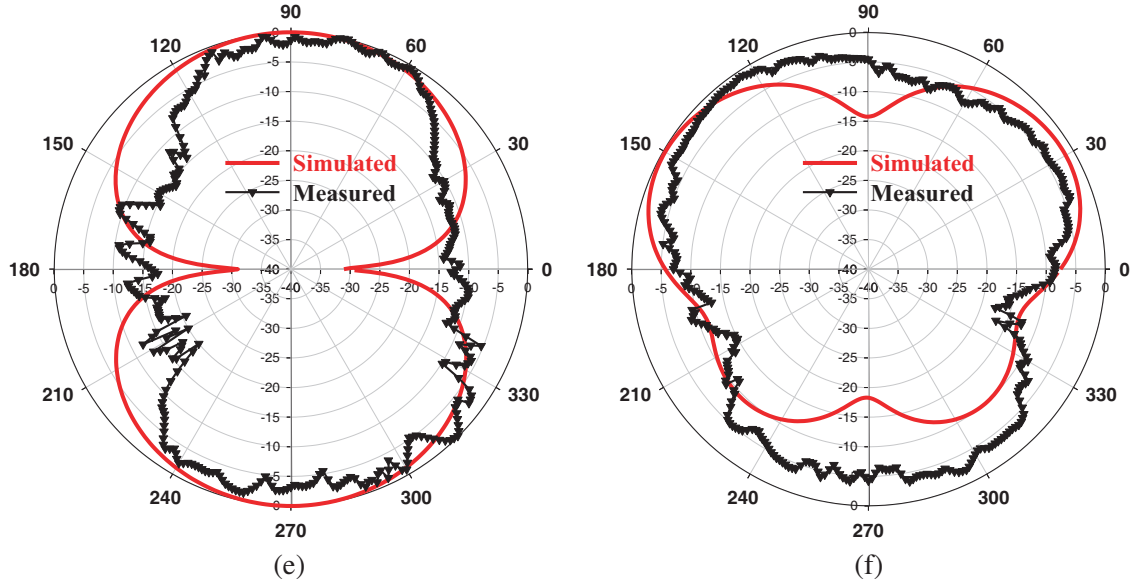


Figure 6. Radiation patterns at different frequencies (3.6, 6 and 9.8 GHz) in the principal planes: (a), (c), (e) E -plane and (b), (d), (f) H -plane.

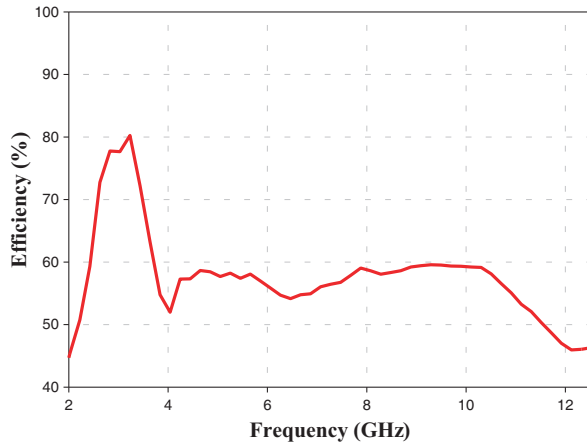


Figure 7. Simulated efficiency curve over the entire band.

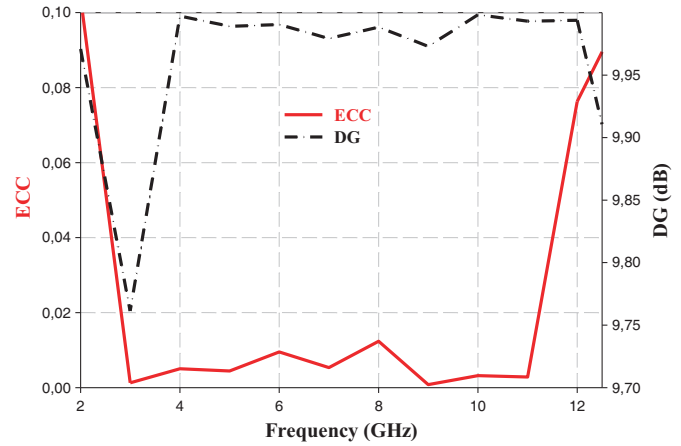


Figure 8. Simulated ECC and diversity gain (DG) curves.

where ECC denotes the envelope correlation coefficient; i and j are the number of ports.

$$ECC(i, j) = \frac{\left(\oint (X_{PR} E_{\theta i}(\Omega) E_{\theta j}^*(\Omega) P_{\theta}(\Omega) + E_{\phi i}(\Omega) E_{\phi j}^*(\Omega) P_{\phi}(\Omega)) d(\Omega) \right)^2}{\oint (X_{PR} G_{\theta i}(\Omega) P_{\theta}(\Omega) + G_{\phi i}(\Omega) P_{\phi}(\Omega)) d(\Omega) \oint (X_{PR} G_{\theta j}(\Omega) P_{\theta}(\Omega) + G_{\phi j}(\Omega) P_{\phi}(\Omega)) d(\Omega)} \quad (2)$$

where X_{PR} denotes the cross-polarization power ratio of the propagation environment. In the formula above, $G_{\theta}(\Omega) = E_{\theta}(\Omega) E_{\theta}^*(\Omega)$ and $G_{\phi}(\Omega) = E_{\phi}(\Omega) E_{\phi}^*(\Omega)$ are the power patterns of θ and ϕ polarizations, respectively. $P_{\theta}(\Omega)$ and $P_{\phi}(\Omega)$ denote the angular density functions of the θ and ϕ polarizations, respectively.

$E_{\theta i}(\Omega)$ and $E_{\theta j}(\Omega)$ are the electric field patterns of the i th and j th antenna elements in the θ polarization, respectively. $E_{\phi i}(\Omega)$ and $E_{\phi j}(\Omega)$ are the electric field patterns of the i th and j th antenna elements in the ϕ polarization, respectively.

The diversity gain can be calculated from the ECC by the below approximate formula [15–17].

$$DG = 10\sqrt{(1 - |\rho|^2)} \quad (3)$$

where ρ is the complex cross correlation coefficient, and $|\rho|^2 = ECC$.

Observing Figure 8, the antenna has a very low ECC from the radiation patterns (3D) in the whole band ($ECC < 0.057$), which implies that the designed MIMO antenna has a low correlation and a high diversity gain (more than 9.78 dB).

3.7. Total Active Reflection Coefficient and Total Channel Capacity Loss

The analysis of the total active reflection coefficient is very important for good MIMO antenna performance. It can be determined using the S -parameters [18, 19]. In the case of a two-port MIMO antenna, the TARC is defined as follows:

$$TARC = \sqrt{\frac{|S_{11} + S_{12}e^{j\theta}|^2 + |S_{21} + S_{22}e^{j\theta}|^2}{2}} \quad (4)$$

where “ θ ” is the input feeding phase angle of each excited signal in a MIMO system and varied from 0° to 180° . From Figure 9(a), the TARC value of the proposed MIMO antenna at $\theta = 90^\circ$ is less than -10 dB across the UWB, which meets the criteria for MIMO performance. The total channel capacity loss for this case is calculated using a 2×2 correlation matrix as shown in equation Eq. (5) [20]. This metric measures the degradation of the MIMO channel capacity due to the influence of cross-coupling between the signals received in an antenna array. For a MIMO system, the maximum acceptable value of CCL should be less than 0.4 bits/s/Hz.

$$CCL = -\log_2 \det(\psi^R) \quad (5)$$

where ψ^R represents the correlation matrix of the receiving antennas and is given mathematically as:

$$\psi^R = \begin{bmatrix} \rho_{11} & \rho_{12} \\ \rho_{21} & \rho_{22} \end{bmatrix} \quad (6)$$

where $\rho_{ii} = 1 - \left| \sum_{n=1}^M S_{in}^* \times S_{ni} \right|$ and $\rho_{ij} = - \sum_{n=1}^M S_{in}^* \times S_{nj}$ for $ij = 1$ and 2 . ρ_{ii} and ρ_{ij} are the correlation coefficients.

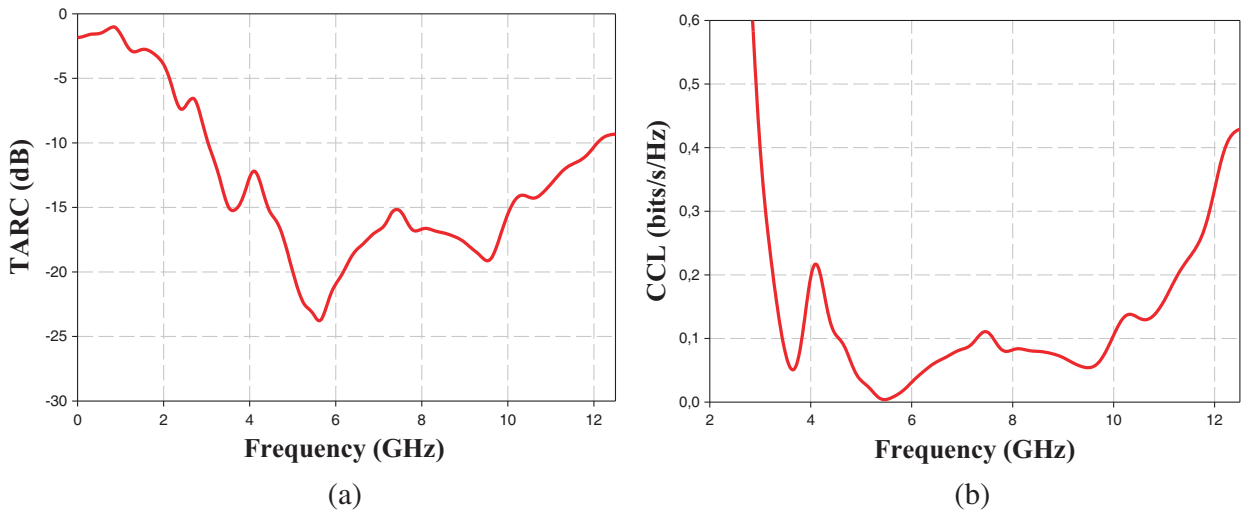


Figure 9. Simulated TARC and CCL_{Total} curves: (a) TARC and (b) CCL_{Total} .

For more realistic results, the transmission power losses due to the TARC coefficient are also considered. Therefore, the global capacity loss of the channel [20] is in the following form:

$$CCL_{Total} = -2\log_2(1 - TARC^2) - \log_2 \det(\psi^R) \quad (7)$$

As depicted in Figure 9(b), the simulated CCL_{Total} is less than 0.25 bits/s/Hz in the entire UWB, indicating acceptable antenna performance to achieve reliable transmission rate in a rich scattering environment.

4. PERFORMANCE COMPARISON

To highlight the novelty of the design presented in this paper, Table 3 lists the performance comparison of this paper with the antennas proposed in References [21–25], where the proposed antenna has a more compact size, wider operational bandwidth, and low envelope correlation coefficient compared to the antennas mentioned in this table. In addition, the antenna has an isolation of more than 16.5 dB in the ultra-wideband, which is better than the antennas mentioned in the literature [23, 25]. Although the isolation of the antenna in the literature [21, 22, 24] is better than the antenna designed in this paper, the size of these antennas is near the twice of of the antenna in this paper.

Table 3. Performance comparison with previous published literature.

Ref. No.	Size in term of (mm ²)	BW range (GHz)	BW (GHz)	Isolation (dB)	ECC	Efficiency
P.S	46 × 46	3.1 ~ 11.7	8.6	16.5	< 0.057	59%
[21]	50 × 80	4.183 ~ 6.584	2.399	17	< 0.0568	80%
[22]	93 × 47	3.1 ~ 10.6	7.5	31	-	70%
[23]	110 × 54	5 ~ 7.3	2.3	16	-	80%
[24]	64 × 45	2 ~ 10.6	8.6	31	< 0.02	
[25]	58 × 45	2.76 ~ 10.75	7.99	15	< 0.01	80%

P.S = Proposed structure

5. CONCLUSION

In this paper, a compact CPW-fed two-port MIMO antenna with high performance is proposed for UWB applications. In the ground plane, a vertical T-shaped neutralization line is added between the two monopole radiators to enhance the isolation, which provides a good choice for portable ultra-wideband communication systems. The proposed structure has a wider operational bandwidth, which increases the channel capacity and data rates of individual links between the base station and mobile users. In addition, the antenna has better diversity performance in terms of low ECC (< 0.57) high DG (≥ 9.78), low CCL_{Total} (≤ 0.25 bits/s/Hz) and TARC (≤ -10 dB).

ACKNOWLEDGMENT

This work was partially supported by Faculty of Sciences, under Information Systems and Telecommunications Laboratory, Abdelmalek Essaâdi University, Tetuan, Morocco, Supervised by Professor Mohsine Khalladi.

REFERENCES

1. Wu, A., M. Zhao, P. Zhang, and Z. Zhang, "A compact four-port MIMO antenna for UWB applications," *Sensors*, Vol. 22, No. 15, 2022.

2. Tirado-Méndez, J. A., H. Jardón-Aguilar, A. Rangel-Merino, L. A. Vasquez-Toledo, and R. Gómez-Villanueva, “Four ports wideband drop-shaped slot antenna for MIMO applications,” *Journal of Electromagnetic Waves and Applications*, Vol. 34, No. 9, 1159–1179, 2020.
3. Sohi, A. K. and A. Kaur, “UWB aperture coupled circular fractal MIMO antenna with a complementary rectangular spiral Defected Ground Structure (DGS) for 4G/WLAN/radar/satellite/International Space Station (ISS) communication systems,” *Journal of Electromagnetic Waves and Applications*, Vol. 34, No. 17, 2317–2338, 2020.
4. Addepalli, T. and V. R. Anitha, “Design and analysis of a novel compact spanner-shaped ultra-wideband antenna for MIMO systems,” *Int. J. Commun. Syst.*, Vol. 34, No. 5, 1–13, 2021.
5. Dkiouak, A., A. Zakriti, M. El, H. Elftouh, A. Mchbal, and A. Zakriti, “Design of CPW-fed MIMO antenna for ultra-wideband communications,” *Procedia Manuf.*, Vol. 46, No. 2019, 782–787, 2020.
6. Thakur, E., N. Jaglan, and S. D. Gupta, “Design of compact triple band-notched UWB MIMO antenna with TVC-EBG structure,” *Journal of Electromagnetic Waves and Applications*, Vol. 34, No. 11, 1601–1615, 2020.
7. Dkiouak, A., A. Zakriti, and M. El Ouahabi, “Design of a compact dual-band MIMO antenna with high isolation for WLAN and X-band satellite by using orthogonal polarization,” *Journal of Electromagnetic Waves and Applications*, Vol. 34, No. 9, 1254–1267, 2019.
8. El Ouahabi, M., A. Zakriti, M. Essaaidi, A. Dkiouak, and H. Elftouh, “A miniaturized dual-band MIMO antenna with low mutual coupling for wireless applications,” *Progress In Electromagnetics Research C*, Vol. 93, 93–101, 2019.
9. Desai, A., M. Palandoken, J. Kulkarni, G. Byun, and T. K. Nguyen, “Wideband flexible/transparent connected-ground MIMO antennas for sub-6 GHz 5G and WLAN applications,” *IEEE Access*, Vol. 9, 147003–147015, 2021.
10. Desai, A., M. Palandoken, I. Elfergani, I. Akdag, C. Zebiri, J. Bastos, J. Rodriguez, and R. A. Abd-Alhameed, “Transparent 2-element 5G MIMO antenna for sub-6 GHz applications,” *Electronics*, Vol. 11, No. 2, 251, 2022.
11. Dkiouak, A., A. Zakriti, M. El Ouahabi, A. Zugari, and M. Khalladi, “Design of a compact MIMO antenna for wireless applications,” *Progress In Electromagnetics Research M*, Vol. 72, 115–124, 2018.
12. Du, C., Z. Zhao, X. Wang, and F. Yang, “A compact CPW-fed triple-band MIMO antenna with neutralization line decoupling for WLAN/WiMax/5G applications,” *Progress In Electromagnetics Research M*, Vol. 103, 129–140, 2021.
13. Dama, Y. A. S., S. M. R. Jones, D. Zhou, N. J. Mcewan, M. B. Child, and P. S. Excell, “An envelope correlation formula for (N, N) MIMO antenna arrays using input scattering parameters, and including power losses,” *Int. J. Antennas Propag.*, Vol. 2011, 7, August 2011.
14. Irene, G. and A. Rajesh, “Review on the design of the isolation techniques for UWB-MIMO antennas,” *Adv. Electromagn.*, Vol. 7, No. 4, 46–70, 2018.
15. Sharma, A. and A. Biswas, “Wideband multiple-input-multiple-output dielectric resonator antenna,” *IET Microwaves, Antennas Propag.*, Vol. 11, No. 4, 496–502, 2017.
16. El Omari El Bakali, H., A. Zakriti, A. Farkhsi, A. Dkiouak, and M. El Ouahabi, “Design and realization of dual band notch UWB MIMO antenna in 5G and Wi-Fi 6E by using hybrid technique,” *Progress In Electromagnetics Research C*, Vol. 116, 1–12, 2021.
17. Adamu, H. J., G. Adnan, J. L. Xue, A. Abdu, S. Saminu, M. S. Abubakar, and M. J. Adamu, “Design of a compact UWB/MIMO antenna with high isolation and gain,” *Proc. 2020 IEEE Work. Microw. Theory Tech. Wirel. Commun. MTTW 2020*, 72–75, 2020.
18. Chae, S., S. Oh, and S. Park, “Analysis of mutual coupling, correlations, and TARC in WiBro MIMO array antenna,” *IEEE Antennas and Wireless Propagation Letters*, Vol. 6, 122–125, 2007.
19. Fritz-Andrade, E., H. Jardon-Aguilar, and J. A. Tirado-Mendez, “The correct application of total active reflection coefficient to evaluate MIMO antenna systems and its generalization to N ports,” *Int. J. RF Microw. Comput. Eng.*, Vol. 30, No. 4, 1–10, 2020.

20. Valderas, D., P. Crespo, and C. Ling, "UWB portable printed monopole array design for MIMO communications," *Microwave and Optical Technology Letters*, Vol. 52, No. 4, 889–895, 2010.
21. Jehangir, S. S. and M. S. Sharawi, "A miniaturized UWB bi-planar Yagi-like MIMO antenna system," *IEEE Antennas Wirel. Propag. Lett.*, Vol. 16, 2320–2323, 2017.
22. Radhi, A. H., R. Nilavalan, Y. Wang, H. S. A. Raweshidy, A. A. Eltokhy, and N. A. Aziz, "Mutual coupling reduction with a wideband planar decoupling structure for UWB MIMO antennas," *Int. J. Microw. Wirel. Technol.*, Vol. 10, No. 10, 1143–1154, 2018.
23. Talha, M. Y., K. J. Babu, and R. W. Aldhaheri, "Design of a compact MIMO antenna system with reduction mutual coupling," *Int. J. Microw. Wirel. Technol.*, Vol. 8, No. 1, 117–124, 2016.
24. Jaglan, N., S. D. Gupta, E. Thakur, et al., "Triple band-notched mushroom and uniplanar EBG structures based UWB MIMO/diversity antenna with enhanced wideband isolation," *AEU — Int. J. Electron. Commun.*, Vol. 90, 36–44, 2018.
25. Jaglan, N., S. D. Gupta, B. K. Kanaujia, et al., "Triple band notched DG-CEBG structure-based UWB MIMO/diversity antenna," *Progress In Electromagnetics Research C*, Vol. 80, 21–37, 2018.